The Interaction of Xe and Xe + K with Graphene

Aaron Bostwick,[1] J. L. McChesney,[1,2] Taiuske Ohta,[1,3] Konstantin V. Emtsev,[4] Thomas Seyller,[4] Karsten Horn,[3] and Eli Rotenberg[1]

[1]*Advanced Light Source, Lawrence Berkeley National Laboratory, Berkeley, California, USA*
[2]*Montana State University, Bozeman, Montana, USA*
[3]*Fritz-Haber-Institut der Max-Planck-Gesellschaft, Berlin, Germany*
[4]*Institut für Physik der Kondensierten Materie, Universität Erlangen-Nürnberg, Erlangen, Germany*

(Dated: November 7, 2009)

We have investigated the electronic properties of monolayer graphene with adsorbed layers of xenon or potassium, or a combination of the two. The formation of the first Xe layer is characterized by a dipole polarization which is quenched by a second Xe layer. By comparing K on Xe on graphene to K on bare graphene, we determine the K contribution to trigonal warping and mass renormalization due to electron-phonon coupling. The former is found to be small but significant, while the latter is shown to be negligible.

PACS numbers:

INTRODUCTION

The doping-dependent properties of graphene, a single layer of carbon atoms in a graphite-like honeycomg lattice, are important both fundamentally and technologically[1]. We have previously shown that the doping can be readily accomplished by adsorbing K atoms, upon which we observed enhancements to the electron-electron and electron-phonon interactions[2]. In contrast, many studies have performed the doping through gating the graphene in a field-effect device geometry[3, 4]. So it is important to understand whether any of the effects induced by potassium are related to the proximity of the dopant ions or are intrinsic to doped graphene.

Here we separate the effects of K atoms from the doping-induced effects by comparing K adlayers on graphene with or without a film of Xe atoms condensed onto the graphene at low temperatures. We find that the doping of the graphene proceeds in either case as a function of K deposition, but when K is diplaced by Xe atoms, we observe several interesting features: (1) the carbon bands are distinctly broadened due to scattering through the Xe layer; (2) the trigonal warping of the carbon bands is reduced, suggesting that some of the warping observed for graphene/K is due to the K Coulomb potential; (3) there is no detectable change in the mass renormalization of the graphene bands when Xe is present, suggesting that the anomalously large electron-phonon coupling previously reported[2, 5] is not due to the influence of the K donor ions.

Although the motivation of this study is to explore the strong chemical interaction of graphene with K, the bonding of graphene to Xe is also interesting. Xe atoms are bonded only weakly to graphene through hybridization of Xe $5p$ and $6s$ states to the C π bands, $\sim$ -4 eV below and 5 eV above E_{F}, resp., with no ionic charge transfer between Xe and graphene [6]. The bonding to the substrate is weak, on the order of the interatomic Xe interaction, and the phase diagram of Xe on graphite is complicated and well-characterized [7]. As in bulk graphite and Xe crystals, a significant contribution to the bonding by van der Waals interaction could be expected; such interactions figure prominently in interfaces between organic conductors and metals, and are difficult to calculate[8]. The Xe on graphene system can therefore be a model for such weakly-bonded systems.

Graphene was prepared at the surface of SiC(0001) by the usual UHV annealing method [9]. Our method of preparation and details of the clean and K-doped band structure (without Xe) are further described in Refs. [2, 5, 10]. Such samples consist of a conductive graphene layer on top of a graphene-like, but insulating, buffer layer with $6\sqrt{3} \times 6\sqrt{3}$ symmetry[9, 11, 12]. Samples at temperature $T < 20$ K were exposed to Xe gas to adsorb the initial rare-gas film, under which conditions 3-dimensional Xe is known to condense in the related Xe/graphite system[7]. Afterwards, K was deposited from a commercial source (SAES Getters). The amount of K deposited was such that in both cases the charge transferred to the graphene is the same. This was accomplished by monitoring the band structure in real time during the K deposition, so that K deposition could be terminated when the desired Fermi surface radius was achieved.

CONDENSATION OF XE FILM

Fig. 1 shows the Xe $4d$ core level spectrum acquired as a function of time during the condensation of the Xe rare-gas film. A total of forty eight spectra were acquired, starting from clean (spectrum #1) up to ~ 1.77 layers (#48), the latter thickness obtained assuming an electron escape depth of 3.5Å at the kinetic energy used [13], a layer thickness of 3.6Å for fcc Xe(111), and full coverage of the first monolayer. In addition to the core level spectrum, a valence band spectrum along the $\overline{\mathrm{GKM}}$ direction of the graphene Brillouin Zonewas acquired for each dosing step. The initial Xe exposure (spectra #1-22, 0.24L total) was accomplished at Xe pressure 5×10^{-10} Torr while the remaining spectra (#23-48, 5.2L additional) were collected in a Xe pressure ten times greater. Each cycle consisting of a core-level and valence band spectra was acquired in 40 s.

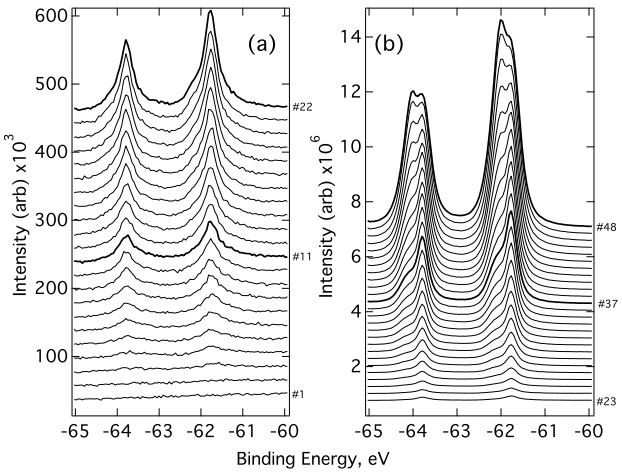

FIG. 1: A series of Xe 4d spectra for different coverages Xe on graphene. (a) spectra #1-22, which start from the clean surface and were obtained for $P = 5 \times 10^{-10}$ T. (b) spectra #20-48 which go up to ~ 1.95 layers and were obtained for $P = 5 \times 10^{-9}$ T.

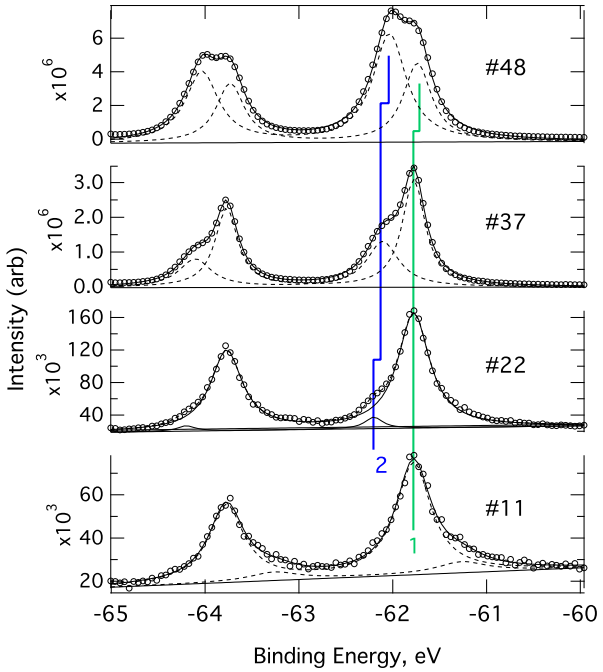

FIG. 2: A series of Xe 4d spectra for different coverages Xe on graphene. (a) spectra #1-22, which start from the clean surface and were obtained for $P = 5 \times 10^{-10}$ T. (b) spectra #20-48 which go up to ~ 1.95 layers and were obtained for $P = 5 \times 10^{-9}$ T.

Four selected core level spectra are plotted, together with least-squares curve-fits are shown in Fig. 2. All the core-level spectra were fitted with Voigt spectra (Lorentzian peaks with Gaussian broadening) with fixed Gaussian width of 25 meV (representing the instrumental resolution), much smaller than the peak widths observed. Judging by the good quality of all the fits, it appears such a small Gaussian is well-justified, and that the lifetime of the Xe core levels is reflected by the Lorentzian widths, and not by any significant amount of inhomogeneous broadening.

Fig. 2 shows that in the initial phase of condensation (spectrum #11 of Fig. 1), the Xe is adsorbed mainly into a single species ("peak 1"). Compared to the spectra that follow, the core-level lifetime is relatively short, as indicated by a large Lorentzian width. We note that the peaks in this stage are slightly asymmetric to lower binding energy (BE), and that this asymmetry could be accounted for by a small core level peak shifted about 0.5 eV from the main peak. It is not clear how to interpret this peak, since chemical interaction of the Xe with the graphene seems unlikely. (Due to the limited statistics available, a clear trend in the width or area of this peak could not be observed.)

The most likely explanation is that the low-BE feature corresponds to Xe preferentially bound at grain boundaries or exposed regions of the buffer layer under the graphene, which can be found for samples prepared similarly[14]. In this scenario, we do not associate the energy shift with a chemical shift (since the chemical interactions are assumed negligible) but rather with changes in the final-state screening of the core hole. Such screening effects typically increase the kinetic energy of the outgoing photoelectron according to the strength of the local dielectric constant, which may be higher due to the closer proximity to the SiC substrate. In this scenario, the shifted peak vanishes relative to the main peak because it represents a small minority of the sample whose signal is eventually dominated by the main peak.

We also note some interesting trends in the linewidths in the early phases of adsorption. At its first appearance, peak 1 is very broad, but at the later coverages, it has sharpened considerably and its width has stabilized. This trend is evident in Fig. 3, which plots the Lorentzian widths, peak positions, and peak areas for all of the spectra. We expect that the first layer Xe atoms are initially isolated, followed by a transition to nucleated monolayer islands, and we associate this transition to the sharp change in linewidth before spectrum #11. This transition in the lifetimes is very difficult to explain, since it implies either a strong change in valence – which we reject due to the weak chemical interaction– or else associated with the vibrational motion of the Xe atoms. The latter seems more likely, although the associated change in binding energy of peak 1 suggests a more complicated explanation.

At the next stages of condensation (spectra #22, 37), peak 1 is now accompanied by a second peak ("peak 2") to higher BE, which we identify with second-layer Xe atoms, similar to what has been seen for Xe multilayers on metals [15]. The BE shift between peaks 1 and 2 is not due to chemical interaction, but the different screening environment seen by the different Xe layers. It must be that the SiC + buffer layer substrate is more polarizable than the first Xe layer, hence the first Xe layer's photoelectrons have a significant energy increase com-

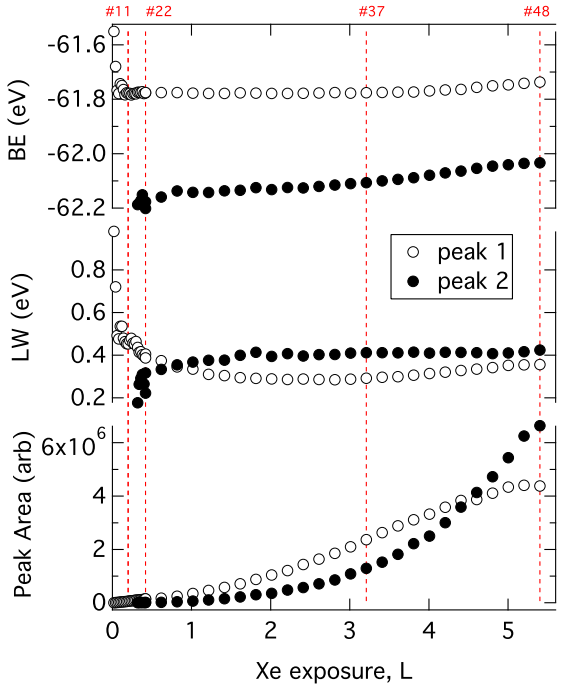

FIG. 3: Core-level parameters for peaks 1 and 2 (see Fig. 1) as a function of Xe coverage. (upper) Binding Energy (BE) (middle) Lorentzian Width (LW), and (bottom) Peak area as a function of Xe exposure at $T = 20$K in Langmuir.

pared to the second layer's photoelectron [15, 16].

The opposite trends in linewidth are observed for the early adsorption of second layer Xe: peak 2 appears at first sharp, and then broadens, and there is an associated decrease in the second layer BE. At higher coverage, between spectra #22-37, the first layer's BE is stable, while second layer's BE continuously decreases. In this same range, though, the first layer's core level lifetime is continously increasing, while the second layer's lifetime remains stable for this and higher coverages. Finally, at higher coverages, past spectrum #37, both first layer's BE abruptly decreases, while the second layer's core level BE abruptly increases its rate of decrease.

We generally expect changes in BE to be related to local screening effects [15, 16] but we should also consider the possibility that there are small changes in local field due to polarization of the Xe layers. Such polarization effects were observed by work-function changes in Xe on graphite in experiments[17] and in model calculations[18]. We now show that such changes could be accurately measured by angle-resolved photoemission spectroscopy measurements (ARPES) of the graphene bands.

Simultaneous measurements of the band structure with the core-levels were obtained, and selected valence band spectra are shown in Fig. 4 for the $\overline{\mathrm{GKM}}$ direction of the graphene Brillouin Zone. Along these directions, only one of the two bands at K is shown because of a matrix element effect [10, 19, 20]. The remaining band is shown to change little in accord with the negligible interaction between Xe and the occupied C π states already discussed for Xe on graphite [6, 21]. In particular, we can detect no shift of the band along the energy axis (i.e. no shift in E_{F}), which would indicate charge transfer due to chemical bond formation between C and Xe atoms.

We analysed these data by curve-fitting cuts at constant BE (so-called momentum-distribution curve (MDC) fitting) to Gaussian-broadened Lorentzians. We fixed the Gaussian width to .012 $\mathrm{\AA}^{-1}$ set by the instrumental resolution, and plotted the resulting peak areas and Lorentzian widths (LW) as a function of Xe coverage.

The most prominent changes to the bands are the reduction in their intensity (not visible in Fig. 4 where the grayscales have been individually normalized), as shown in Fig. 5 for the MDCs at E_{F}. There is a clear breakpoint where the intensity decreases more rapidly, starting around spectrum #37. The LW has a significant increase at the same breakpoint (although the data show some scatter). These changes would conventionally indicate the increased attenuation of the graphene bands by the nucleation of second-layer Xe. But we have seen from the core-level data that second layer formation had begun significantly earlier, so we conclude instead that there must be an electronically-driven transition in the Xe layer which abruptly increases the scattering rate of the final state electrons (at energy around the photon energy 95 eV). This could be related to the formation of Xe-derived bands at high energy above E_{F}, for example, which occur when the second layer undergoes a transition from individual atoms to ordered clusters.

The proposed electronic transition is correlated to a small sideways shift in the bands, reflected in a plot of the relative position of the Fermi momentum Δk_{F} in Fig. 5. Since the graphene band is a well-directed narrow beam, such k-shifts can be attributed to the refraction of the outgoing electrons by the change in surface potential barrier associated with a surface dipole layer at the graphene-Xe interface or at the Xe surface. Changes to the work function can be related to this angular shift in the outgoing photoelectron wave through the standard relation between the Fermi momentum and emission angle:

$$k_F = \sqrt{\frac{2m}{\hbar^2}(h\nu - \Phi)}\sin\theta \qquad (1)$$

where m is the free electron mass, Φ is the work function, $h\nu$ is the photon energy, and θ is the angle of emission relative to the surface normal. Since the lattice constant is fixed (we can hardly imagine an influence on the C lattice constant since the in-plane bonding of Xe is so weak) and hence k_F is fixed, any apparent increase in $|k_F|$ is attributable to an increase in $|\theta|$ as Φ increases. Because the angular resolution is high (on the order of 0.1° or better), we can be sensitive to very small work-function changes, and we can be sure that the change in surface dipole occurs between the graphene and the detector, since the band originates in the graphene layer.

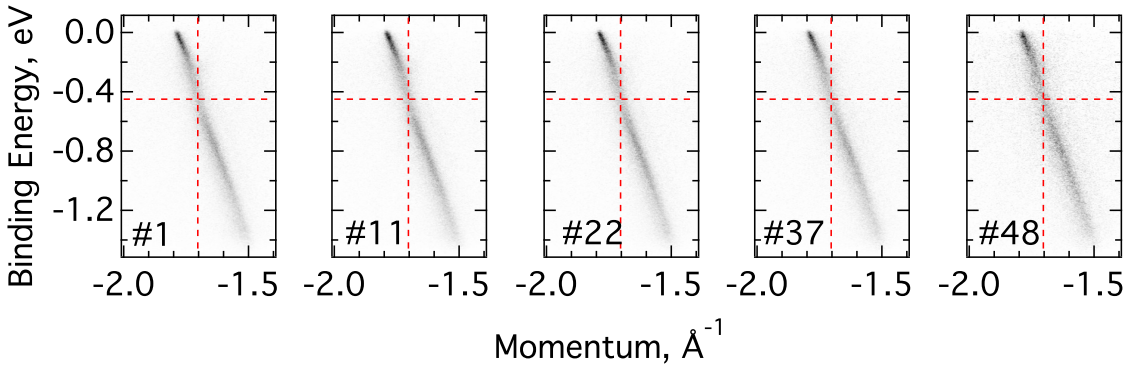

FIG. 4: The graphene band structure for corresponding to the core level spectra numbered as indicated; since the data are acquired during the continuous accumulation of Xe, actual coverages are midway between core level spectra $\#n$ and $\#n+1$.

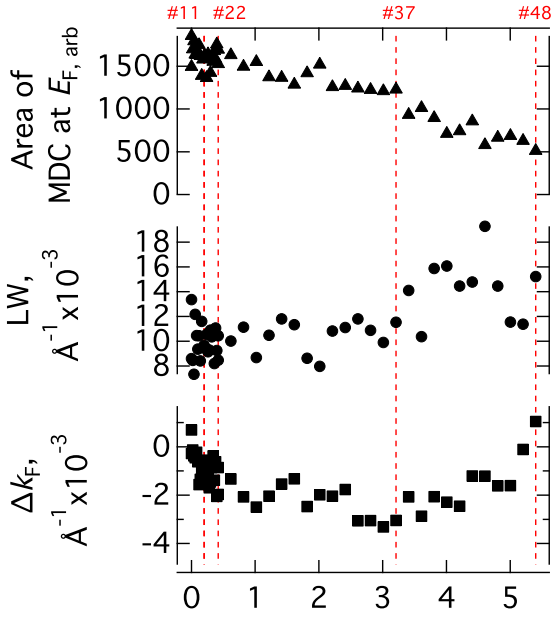

FIG. 5: Band structure parameters as a function of Xe coverage. (upper) the peak area of the momentum distribution curve at $E_{\rm F}$ (middle) the Lorentzian full width (bottom) the Fermi momentum crossing $k_{\rm F}$ for spectra numbered as in Fig. 1.

In Fig. 5 we see that the Fermi wavevector $k_{\rm F}$ first decreases (i.e. the bands in Fig. 4 shift slightly to the left up to spectrum #37) linearly up to 3L coverage, and then reverses. The reversal takes place around the same coverage as the increased scattering rate. The direction of the shift implies a surface dipole moment of the first Xe layers, in which negative charge is driven away from the substrate side towards the vacuum, and corresponds to a total work function increase of about 200 meV at 3L coverage. A similar, but smaller, increase in Φ has been previously observed[17] and calculated[18].

The positive work function shift corresponds to a dipole within the first layer Xe atoms pointed towards the substrate, and is thought to stabilize the Xe - C bond [18]. The fact that the shift is about double that in the Xe-graphite system suggests an even stronger bond to graphene/SiC than graphite, possibly due to the relatively large electron population in the former.

These results are interesting, and show that the photoelectron beams from graphene, being very narrow in angular space, can be a useful probe of subtle overlayer charge distributions. These charge distributions, such as the derived change in surface dipole strength, can only be inferred from work-function measurements, which measure the total charge distribution across the entire film/near surface region of the substrate.

What is more, as the second layer Xe coverage becomes important beyond 3 L exposure, the total Xe dipole moment is reversed, suggesting either that the second layer has a reverse dipole moment compared to the first layer, or else, that the dipole moment in the first layer diminishes towards zero as the second layer is formed. The latter explanation is more likely, because of the associated changes in BE and LW of peak 1 in correspondence to the reduction in surface dipole moment.

The increased core-hole lifetime of peak 1 between 0.25L and 3L followed by its decrease beyond 3L is now explained as due to the reconfiguration of the Xe valence orbitals, which in the polarized state must have a lower probability of decay into the Xe $4d$ core hole. Peak 2's lifetime trend is also naturally explained by a simple model: at low coverage, the isolated second layer atoms may develop a small dipole moment, hance having a long lifetime at low coverage, but the second layer polarization vanishes as these atoms nucleate into larger islands atop the first layer.

Although all the observed core-hole BE and lifetime trends cannot be completely explained without detailed modeling, the data taken together show that the initial stages of Xe adsorption are quite complicated, with screening by the substrate, graphene, and Xe atoms themselves playing important

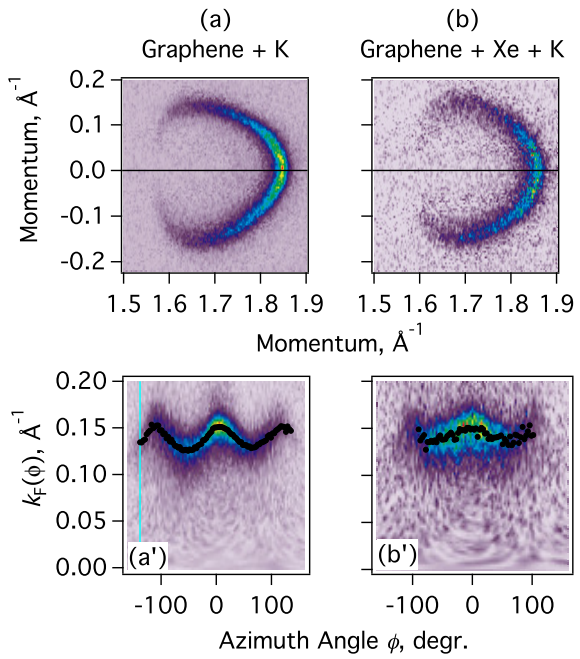

FIG. 6: The Fermi surface of (a) K on graphene and (b) K on Xe on graphene. (a', b') The data, remapped onto rectangular-polar coordinates (k, ϕ) where ϕ is the azimuth angle about the K point of the Brillouin Zone. The symbols show the fitted peak positions.

roles.

DOPING WITH K THROUGH THE XE LAYER

The interaction of potassium with the graphene is interesting because it allows us to control the charge density of the graphene and thereby probe the many-body interactions. Two important questions have arisen: whether the alkali atoms play a role to enhance first, the trigonal warping of the bands [22, 23], and second, the large electron-phonon coupling (or other many-body interactions) in alkali-doped graphene[2].

Fig. 6 shows a comparison of the Fermi surface for two samples, in which the charge carrier density has been significantly increased by doping with K atoms. In sample (a), the K was adsorbed directly onto the graphene layer, while for sample (b), the Xe-coated sample described above was adsorbed with a K layer. In the latter case, we monitored the energy bands of the sample during K growth, terminating the K dosing when the desired Fermi wavelength $k_{\rm F}$ was attained. Both samples had a Dirac crossing energy $E_{\rm D}$~$E_{\rm F}$-0.85 eV, similar to the maximum doping level we have published earlier[2].

The most obvious differences between them is that the sample without Xe has a much stronger departure from circular shape than the one with Xe, i.e. sample (a) has a significantly higher trigonal warping. This subtle effect is made more obvious by mapping the Fermi surface from cartesian space (k_y *vs.* k_x) to rectangular-polar coordinates ($k_{\rm F}$ *vs.* ϕ) where $k_{\rm F}$ is the Fermi crossing momentum and ϕ is the azimuth angle about the K point of the graphene Brillouin Zone where the upper and lower π bands meet.

From this we can conclude that there is a significant amount of trigonal warping when the dopant K atoms are in close proximity to the graphene layer (Fig. 6(a)). When the K atoms are separated from the graphene by the Xe bilayer, the trigonal warping is greatly reduced. To be more quantitative, we fitted the resulting MDCs *vs.* ϕ to locate the peak positions $k_{\rm F}(\phi)$, and the results are plotted as symbols in Fig. 6. The resulting peak positions could be fitted by the function

$$k_{\rm F}(\phi) = k_0 + \alpha\cos(3\phi) \qquad (2)$$

For both samples, the average Fermi surface radius was k_0=0.14 Å^{-1}, but the trigonal warping parameters α were 0.006 and 0.011 Å^{-1}, resp. Thus the influence of the K atoms when near the graphene lattice is to roughly double the trigonal warping. This enhanced trigonal warping is essentially a band structure effect, but not one derived simply from the hybridization of graphene with overlayer bands (as proposed for monolayer of Ca on graphene [24]) nor due to the overlayer K ions' pseudopotential since the overlayer of K atoms is disordered for our conditions[25]. Rather, it should be considered more properly as arising from a disorder-induced potential, in which the K ions are situated uniformly in the honeycomb lattice's hollow site, but randomly among the possible sites.

Although the role of K atoms on the trigonal warping has been speculated upon [22, 23], the present results provide the first clean way to separate the doping from the warping effects of the alkali dopants.

Coming now to the question of the many-body interactions, we have previously estimated the electron-phonon coupling constant λ in K-doped graphene to be in the neighborhood of $\lambda \sim 0.3$ at low doping [2, 5], a value which is around 5 times larger than predicted theoretically[26, 27] for doped graphene (but without the proximity of charged dopant ions). So it is interesting to examine our band structure measurements to see if the large observed value of λ arises from the influence of the dopant atoms.

Fig. 7 shows high-resolution ARPES spectra of the bands for K on graphene without (a) or with (b) the Xe interlayer and have been collected with sufficient resolution to probe the single-particle spectral function

$$A(\mathbf{k},\omega) = \frac{|{\rm Im}\Sigma(\mathbf{k},\omega)|}{\left(\omega - \omega_{\rm b}(\mathbf{k}) - {\rm Re}\Sigma(\mathbf{k},\omega)\right)^2 + \left({\rm Im}\Sigma(\mathbf{k},\omega)\right)^2}, \qquad (3)$$

where $\omega_{\rm b}$ is the bare band (in the absence of many-body effects), and $\Sigma(\mathbf{k},\omega)$ is the self-energy function. We have shown that $\Sigma(\mathbf{k},\omega)$ is approximately $\mathbf{k}$-independent for graphene on SiC[2], and in that situation, Eq. 3 describes a simple Lorentzian function for an MDC at a specific binding energy ω. The linewidth at each MDC ordinarily reflects the inverse mean free path of the photoholes, but in the presence

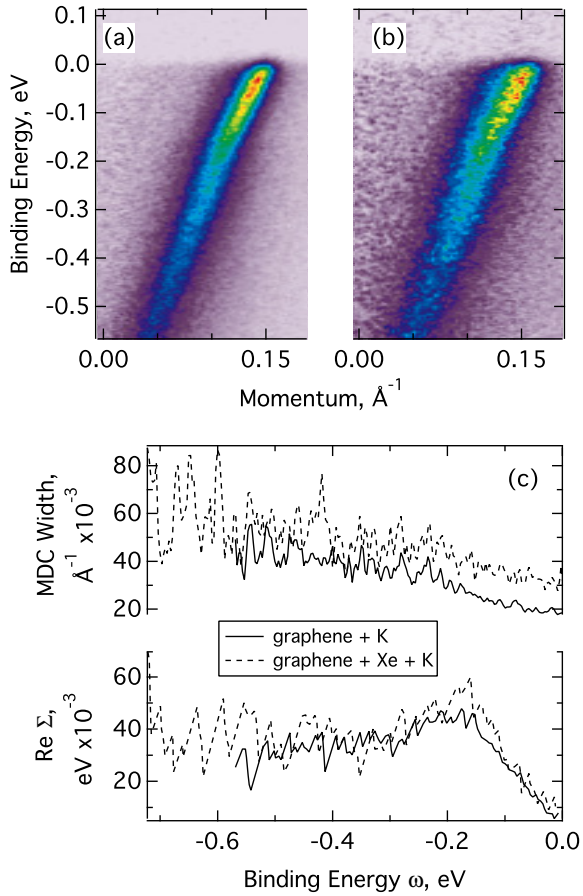

FIG. 7: High-resolution ARPES band structures for (a) K on graphene and (b) K on Xe on graphene. (c) The extracted MDC widths (upper traces) and $\mathrm{Re}\Sigma(\mathbf{k},\omega)$ (lower traces) for the same systems.

of an overlayer can be additionally broadened due to scattering of the photoelectron wave.

We have fitted each MDC in Figs. 7(a,b) and plotted the resulting MDC linewidths in the upper part of Fig. 7c. The two traces show that the energy-dependent linewidths are identical, within a constant offset reflecting merely the final-state scattering of the photoelectrons through the Xe film.

The fitted k-positions of each MDC spectrum yield the momentum $\mathbf{k}$ as a function of ω. By solving the equation

$$\omega(\mathbf{k}) - \omega_{\mathrm{b}}(\mathbf{k}) - \mathrm{Re}\Sigma(\omega) = 0 \qquad (4)$$

with an optimized linear bare band ω_{b}, we can derive the real part of the self energy, which is plotted in Fig. 7c for the two cases (with and without Xe). The bare band was optimized so that causality was obtained (i.e. real and imaginary parts of the self-energy mutually related by Kramers-Kronig transform), and the energy and k-resolution were deconvolved using a procedure to be described elsewhere. Satisfactory analyses were obtained using linear bare bands for the two situations, with slightly differing (by 3%) slopes in line with the difference in trigonal warping discussed above.

The subtle kinks of the bands at ~ 200 meV in Fig. 7a,b is now reflected as the sharp energy dependence of $\mathrm{Re}\Sigma(\mathbf{k},\omega)$ in Fig. 7c, and are shown to be completely equivalent irregardless of whether the doping by K is achieved through direct adsorption onto the graphene or through the Xe interlayer. This, together with the equivalent statement above for the imaginary part, confirms that the electron-phonon coupling we observed is intrinsic to the doped graphene, and not a consequence of the extrinsic interactions with K ions (e.g. through interaction of C π electrons with K vibrations).

The dimensionless electron-phonon coupling constant λ is found from the slope of the real part of the self-energy, and for these samples, a value of $\lambda = 0.26$ is obtained, confirming that there is considerably more coupling near E_{F} than has been calculated. For these samples, the bare band can be well-approximated by a linear function, and therefore distortion of the results near E_{F} by finite bare band curvature[28, 29] can be excluded. The effect of finite temperature broadening and resolution if any is to smooth out the derived self-energy, so in reality the coupling constant could be as high as $\lambda = 0.28$, in line with our earlier estimates[2, 5] for similar doping.

CONCLUSIONS

In these experiments, the bonding of Xe was expected to be simple, and its role as a simple interlayer was proposed to separate out the effects of doping from the proximity of potassium ions. This turned out to be quite successful: In fact, the potassium ions were found to have only the effect of reducing the trigonal warping, but otherwise offering no further renormalization of the bands due to single-particle or many-body interactions. But the story of Xe bonding to graphene turned out to be quite complicated, showing a complicated evolution of the polarization, screening response, and core-hole lifetimes than anticipated. Although some of the effects could be interpreted as arising from the coverage-dependent dipole moments, further experiments and modelling are needed to get a full understanding of the richness of the Xe/graphene phase diagram.

ACKNOWLEDGEMENTS

[1] A. K. Geim and K. S. Novoselov, Nat. Mater. **6**, 183 (2007).
[2] A. Bostwick, T. Ohta, T. Seyller, K. Horn, and E. Rotenberg, Nat. Phys. **3**, 36 (2007).
[3] Y. Zhang, Y. W. Tan, H. L. Stormer, and P. Kim, Nature **438**, 201 (2005).
[4] K. S. Novoselov, E. McCann, S. V. Morosov, V. Fal'ko, M. I. Katsnelson, U. Zeitler, D. Jiang, F. Schedin, and A. K. Geim, Nature **438**, 192 (2005).

[5] A. Bostwick, T. Ohta, J. L. McChesney, T. Seyller, K. Horn, and E. Rotenberg, Solid State Communications **143**, 63 (2007).

[6] X.-R. Chen, X.-L. Zhou, J. Zhu, and Q.-Q. Gou, Phys. Lett. A **315**, 403 (2003).

[7] M. Hamichi, A. Q. D. Faisal, J. A. Venables, and R. Kariotis, Phys. Rev. B **39**, 415 (1989).

[8] P. Sony, P. Puschnig, D. Nabok, and C. Ambrosch-Draxl, Phys. Rev. Lett. **99**, 176401 (2007).

[9] I. Forbeaux, J. M. Themlin, and J. M. Debever, Phys. Rev. B **58**, 16396 (1998).

[10] A. Bostwick, T. Ohta, J. L. McChesney, K. V. Emtsev, T. Seyller, K. Horn, and E. Rotenberg, New J. Phys **9**, 385 (2007).

[11] K. V. Emtsev, T. Seyller, F. Speck, L. Ley, P. Stojanov, J. D. Riley, and R. G. C. Leckey, cond-mat p. 0609383 (2006).

[12] K. V. Emtsev, F. Speck, T. Seyller, L. Ley, and J. D. Riley, Phys. Rev. B **77**, 155303 (2008).

[13] A. Franciosi, A. Raisanen, G. Haugstad, G. Ceccone, and X. Yu, Phys, Rev. B **41**, 7914 (1990), copyright (C) 2009 The American Physical Society Please report any problems to prola@aps.org PRB.

[14] T. Ohta, F. E. Gabalay, A. Bostwick, J. L. McChesney, K. V. Emtsev, A. Schmid, T. Seyller, K. Horn, and E. Rotenberg, New J. Phys. **10**, 023034 (2007).

[15] G. Kaindl, T. C. Chiang, D. E. Eastman, and F. J. Himpsel, Physical Review Letters **45**, 1808 (1980).

[16] E. Rotenberg and M. A. Olmstead, Phys. Rev. B **46**, 12884 (1992).

[17] T. Mandel, M. Domke, G. Kaindl, C. Laubschat, M. Prietsch, U. Middelmann, and K. Horn, Surface Science **162**, 453 (1985).

[18] J. L. F. Da Silva and C. Stampfl, Phys. Rev. B **76**, 085301 (2007).

[19] E. Shirley, L. Terminello, A. Santoni, and F. J. Himpsel, Phys. Rev. B **51**, 13614 (1995).

[20] M. Mucha-Kruczynski, O. Tsyplyatyev, A. Grishin, E. McCann, V. Fal'ko, A. Bostwick, and E. Rotenberg, Phys. Rev. B **77**, 195403 (2008).

[21] B. Grimm, H. Hvel, M. Pollmann, and B. Reihl, Phys. Rev. Lett. **83**, 991 (1999).

[22] A. Gruneis, C. Attaccalite, A. Rubio, D. V. Vyalikh, S. L. Molodtsov, J. Fink, R. Follath, W. Eberhardt, B. Buchner, and T. Pichler, Phys. Rev. B **79**, 205106 (2009).

[23] A. Gruneis, C. Attaccalite, A. Rubio, D. V. Vyalikh, S. L. Molodtsov, J. Fink, R. Follath, W. Eberhardt, B. Buchner, and T. Pichler, Phys. Rev. B **80**, 075431 (2009).

[24] M. Calandra and F. Mauri, Phys. Rev. B **76**, 161406 (2007).

[25] P. Bennich, C. Puglia, P. A. Brhwiler, A. Nilsson, A. J. Maxwell, A. Sandell, N. Martensson, and P. Rudolf, Phys. Rev. B **59**, 8292 (1999).

[26] M. Calandra and F. Mauri, Phys. Rev. Lett. **95**, 237002 (2005).

[27] M. Calandra and F. Mauri, physica status solidi (b) **243**, 3458 (2006).

[28] M. Calandra and F. Mauri, Phys. Rev. B **76**, 205411 (2007).

[29] C.-H. Park, F. Giustino, J. L. McChesney, A. Bostwick, T. Ohta, E. Rotenberg, M. L. Cohen, and S. G. Louie, Phys. Rev. B **77**, 113410 (2008).